

Image-based remapping of spatially-varying material appearance

Alejandro Sztrajman¹, Jaroslav Krivánek², Alexander Wilkie², Tim Weyrich¹

¹University College London, United Kingdom.

²Charles University, Czech Republic.

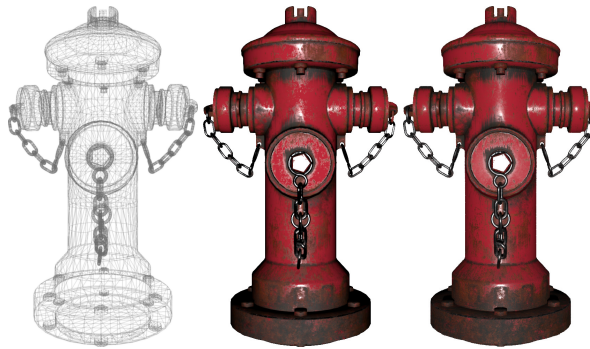


Figure 1: Remapping of material from Blender-Ward (center) to Cycles-GGX (right).

Abstract

BRDF models are ubiquitous tools for the representation of material appearance. However, there is now an astonishingly large number of different models in practical use. Both a lack of BRDF model standardisation across implementations found in different renderers, as well as the often semantically different capabilities of various models, have grown to be a major hindrance to the interchange of production assets between different rendering systems. Current attempts to solve this problem rely on manually finding visual similarities between models, or mathematical ones between their functional shapes, which requires access to the shader implementation, usually unavailable in commercial renderers. We present a method for automatic translation of material appearance between different BRDF models, which uses an image-based metric for appearance comparison, and that delegates the interaction with the model to the renderer. We analyse the performance of the method, both with respect to robustness and visual differences of the fits for multiple combinations of BRDF models. While it is effective for individual BRDFs, the computational cost does not scale well for spatially-varying BRDFs. Therefore, we further present a parametric regression scheme that approximates the shape of the transformation function and generates a reduced representation which evaluates instantly and without further interaction with the renderer. We present respective visual comparisons of the remapped SVBRDF models for commonly used renderers and shading models, and show that our approach is able to extrapolate transformed BRDF parameters better than other complex regression schemes.

1. Introduction

Computer-generated imagery workflows commonly involve a broad range of modelling and rendering tools, each targeting different goals and requirements [SDSG13], and the exchange of data between these tools is hindered by incompatible representations. As a consequence, existing model assets frequently have to be redesigned to be used in other software, resulting in large modelling overheads. This is particularly true in the case of material models. So far, a great number of BRDF models has been developed for appearance

representation, but a lack of a standardisation and renderer-specific implementation details lead to visual deviations even between identically named reflectance models.

The current abundance of BRDF models reflects that no single model is able to realistically reproduce the full range of available measured materials [BLPW14, GGG*16]. However, for a given material, represented using one model, it is often possible to find a new set of parameters which approximates its appearance with a different model. Many existing rendering systems support such

remapping of material parameters to address the incompatibility between models, and be it to remain backwards-compatible to older version of their software [PJH16, Cor17]. That said, these remappings are often based on manually determined, or heuristic relations between the functional shapes of the models, or incur oversimplifications by assuming one-to-one correspondence between individual parameters of both models. The problem is exacerbated by popular renderers and graphics engines using their own shading models [May17, Unr17, Uni17].

An automatic solution to this problem needs to consider the constraints of the real-world scenario where a material is interchanged between different third-party renderers. In this situation, we do not have access to the implementation of the shaders, only to the model parameters and the resulting renderings. To address this problem, we present an image-based method for the remapping of BRDFs which works for closed-source renderers, assuming no knowledge of the model implementations. We analyse the robustness of the method applied to a set of BRDF models, and we discuss common issues and strategies to improve the stability of the method in different types of materials.

In addition, we present a regression scheme to generate a reduced representation of the transformation which evaluates instantly and without further interaction with the renderer, allowing the fast remapping of entire parameter texture maps. We show visual comparisons of the remapping of spatially-varying BRDF models (SVBRDF) that illustrate the ability of our approach to provide a close match between different renderers, even when remapping between very different shading models.

2. Related Work

2.1. Reflectance Remapping

Traditionally, appearance modelling dealt with finding reflectance models that would agree well with measured data. Accordingly, a large body of work on fitting of reflectance models exists [Mar98, WLL*08, GGG*16]. In contrast, little academic attention has been paid to the direct translation between BRDF models. Within commercial products, the arguably most prominent software to remap reflectance from one model to another is Allegorithmic’s Substance Painter [All17], a dedicated tool to author appearance for a wide range of target platforms. In order to address the variability in renderer-specific BRDF models and implementations, they contain various export functions that employ manually optimised heuristics to remap BRDF parameters for specific target rendering engines. Manual creation of such heuristics, however, can be costly and does not necessarily lead to optimal results [Dam17].

Another example would be renderers that remap reflectance from older versions’ legacy representations, such as PBRT [PJH16] or Corona [Cor17]. The latter switched from a variant of the Ashikhmin-Shirley BRDF [AS00] to a GGX microfacet BRDF [WMLT07, Bur12] and remaps BRDF specifications by analytically matching the width of the models’ specular lobes [Kri17].

2.2. Appearance Comparison

Quantifying (dis)similarity between two BRDFs is a problem encountered in any BRDF fitting work, and our remapping is no ex-

ception. Ngan et al. [NDM05] follow Lafortune et al. [LFTG97] and employ a simple L_2 distance between cosine-weighted BRDF values. We find that such a metric puts disproportionate emphasis on matching BRDF peaks at the expense of tails, which can result in appearance deviations.

In their follow-up work, Ngan et al. [NDM06] argue for an image-based metric, where the dissimilarity between two BRDFs is modelled as the difference between the rendered images with the respective BRDFs under natural illumination. Recently, Havran et al. [HFM16] confirmed the validity of the image-based methodology through psychophysical experiments and, furthermore, designed specialised geometries that provide richer information on material properties than the simple sphere used by Ngan et al. We follow this image-based strategy for two reasons: first, it has been repeatedly shown to correlate well with the perceived material differences; second, our setup lends itself well to rendering images using any (unknown) BRDF, whereas obtaining individual BRDF values using an off-the-shelf renderer may be more difficult.

We focus our efforts on finding a remapping scheme which results in parameters that vary smoothly with respect to changes in the source material parameters. For uniform BRDFs this is an expected behaviour of the transformation, and deviations are suggestive of problems in the optimisation, such as finding local minima or output parameters that only look similar in a particular scene setting. For spatially-varying (SV)BRDFs, the smoothness of the mapping is even more important because the material parameters across the surface are computed by interpolation. If the parameters vary abruptly this is likely to produce wrong SVBRDF remappings, even if the appearance of each individual texel is correctly matched.

3. Remapping of Uniform Materials

The process of BRDF remapping is similar in structure to the fitting of BRDFs, where we start with a *target* BRDF model and an initial guess of the parameters, and we want to fit reflectance data, generally measured from a real-world material. This involves the minimisation of the difference between the appearances of the BRDF and the data, performed through non-linear optimisation of the parameters of the BRDF model (Figure 2).

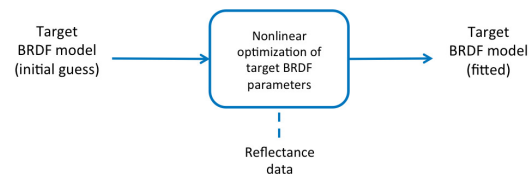


Figure 2: Broad scheme for BRDF fitting.

In the case of BRDF remapping (Figure 3) the scheme is analogous; however, instead of using measured data we are now matching the appearance of the target BRDF model with another *source* BRDF model. In this scheme we assume no direct access to the implementation of the BRDF models. In particular, the target model is assumed to belong to an external renderer in a typical usage scenario of our technique. In order to perform an appearance comparison under

these conditions, we measure the difference in image space, by comparing rendered images of a single scene using each of the two BRDF models.

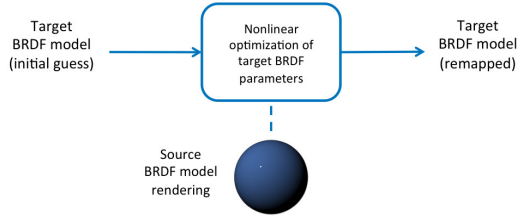


Figure 3: BRDF remapping scheme.

Thus, in each step of the optimisation we only need to be able to generate new renders of this scene with the target BRDF. The image difference is then computed with an L_2 metric in colour space, which is common practice in the context of BRDF fitting [NDM06] (other metrics are used as well, but no single distance metric has emerged as superior choice for general BRDF fitting.)

In the remainder, we will consider three optimisation strategies to remap a (uniform) BRDF specification to parameters of a different model. Section 5 will then present our approach to extend the remapping to spatially-varying appearance.

3.1. Optimisation Strategies

A simple optimisation scheme which attempts to fit all model parameters at once (as shown in Figure 3) often leads to local minima during the optimisation, due to the coupling between the diffuse and specular terms in the model. In Section 4.1 we provide a systematic analysis of the stability of the remapping scheme. In order to improve the stability of the optimisation we test the following two variants of our remapping scheme.

Two-stage remapping

In this scheme the diffuse and specular terms are remapped independently (Figure 4). This is not unlike BRDF fitting to real-world data where diffuse and specular reflectance may be separated optically [DHT*00] or statistically [WMP*06] before conducting separate fits. In our case, it requires source renderings of the diffuse-only, and purely specular components, respectively. In the end we obtain remapped versions of each term which are merged in the remapped target BRDF model.

Three-stage remapping

The two-stage remapping assumes an independence of diffuse and specular terms that might not hold true for some layered materials. The three-stage scheme (Figure 5) recovers the coupling between both terms by using the results of the two-stage scheme as a good starting guess for a subsequent simple remapping that optimises all parameters simultaneously, reducing the chance of falling into local minima.

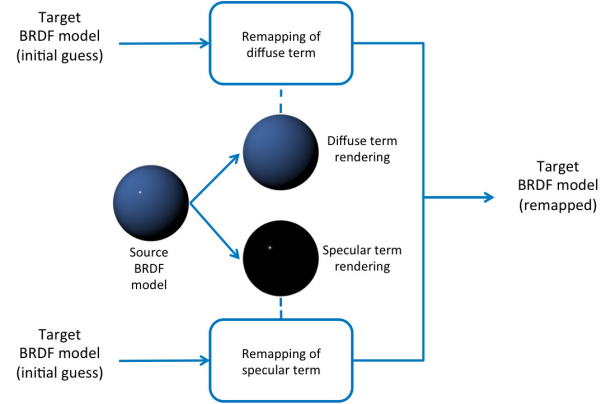


Figure 4: BRDF remapping scheme in two stages. Diffuse and specular components are remapped independently.

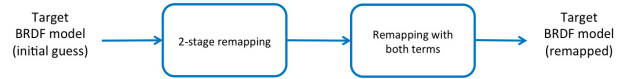


Figure 5: BRDF remapping scheme in three stages.

4. Analysis of Uniform Material Remapping

We tested our approach using three renderers: Mitsuba; Blender’s internal preview renderer; and Cycles, a physically-based renderer that is currently the most commonly used off-line renderer in Blender. Due to differences in how light source intensities are specified across renderers, we further had to match irradiance before remapping an external BRDF to a Mitsuba BRDF. This was done by a global scale determined from the ratio of diffuse-only renderings from the two renderers.

Our uniform BRDF remapping code uses Mitsuba in its inner loop, and thus the optimisation can take source BRDFs from arbitrary renderers while the target BRDF has to be from within Mitsuba. In Section 5.2 we will show that this does not represent a limitation for the remapping, since the transformation to Mitsuba can be used as an intermediate step in a sequence of remappings.

4.1. Uniform Fitting Strategies

We begin by evaluating the three optimisation strategies for remapping of uniform BRDFs which were introduced in Section 3.1. We performed a systematic study of these remapping schemes via an analysis of the robustness of the transformation that links the parameters of the models. We did this for multiple combinations of BRDF models that are available in Mitsuba [Jak10] (Ashikhmin-Shirley, Beckmann, GGX, Phong, Ward). For the sake of brevity, we focus here only on a few of these combinations, to demonstrate a few common effects we encountered when dealing with remapping between different BRDFs within Mitsuba.

We used a simple scene for the image-based appearance comparison: a sphere of radius 2 located in the origin illuminated by a point lightsource. This produces a sampling of only a two-dimensional slice of the BRDF space, that depends on the relative position of the

illumination source. Although we find that the resulting transformations of parameter are not highly dependent on the choice of light position, in Section 5.4 we will discuss its effect on the visual match between BRDF models.

The renderings were generated as colour space HDR images (512×512), and the non-linear optimisation was performed using the Trusted Region Reflective method, enforcing positive values on the remapped parameters.

4.1.1. Conductors

Our analysis of the remapping of conductors comprises 60 materials from Mitsuba’s database. In Figure 6 we show the results for a remapping from Ashikhmin-Shirley (source) to Ward (target). In these implementations the specular terms in both models are described by an RGB specular parameter and the roughness (single-channel), essentially characterising the intensity and the spread of the lobes. We show the remapping of a specular parameter in Ashikhmin-Shirley to an analogous parameter in Ward (both single-channel), for multiple fixed values of roughness. The information provided by the index of refraction in the standard BRDF interface in Mitsuba is here condensed into the Fresnel coefficient F_0 , which can be expressed in its more general form as:

$$F_0 = \frac{(c-1)(c^*-1)}{(c+1)(c^*+1)} \quad (1)$$

where c is the complex index of refraction.

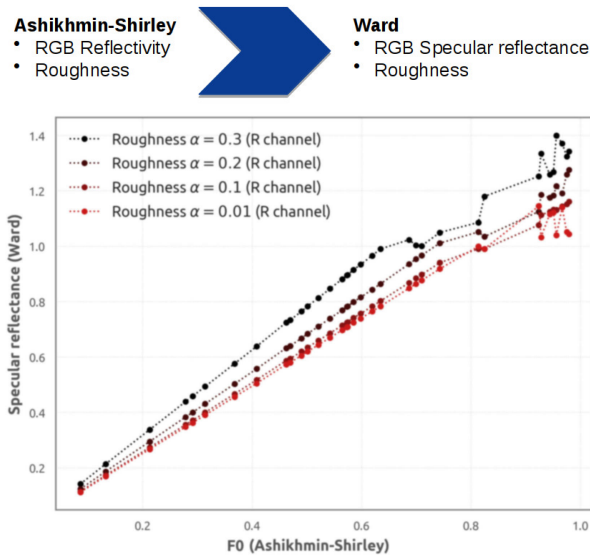


Figure 6: Remapping of conductors from Ashikhmin-Shirley to Ward. Detail of parameters in Mitsuba, and plot of specular reflectance (Ward) vs Fresnel coefficient (AS).

The expected output of the remapping is a smoothly varying correspondence between source and target parameters. In a typical usage case, the user would expect small changes in the source material to correspond to small changes in the exported appearance. We will show that a deviation from this behaviour usually signals

a decreasing capacity of the target model to match the source, or the occurrence of local minima during the optimisation. The stability of the transformation will prove crucial when we deal with the remapping of spatially-varying BRDFs (Section 5) which are reconstructed by interpolation of multiple uniform materials.

In Figure 6 the transformation shows a smooth behaviour for most materials, but exhibits instabilities for parameters which are remapped to specular reflectance > 1 . These can be traced back to this particular implementation of Ward, where the values of specular reflectance are trimmed to avoid energy loss, and is representative of the implementation-dependent behaviour that we may find in renderers. Most of the instabilities we found during our study shared this behaviour of exhibiting well-localised regions in parameter space where the remapping becomes unreliable.

After filtering the unstable cases from Figure 6, Figure 7 shows the results for a round-trip remapping, where we transformed the parameters back to the initial Ashikhmin-Shirley model. The result is a straight line of unitary slope, which shows that in this particular case, the parameters go back to their original values after the two remappings. This speaks for the general robustness of the approach, and indicates that we generally can recover the original appearance after a remapping takes place.

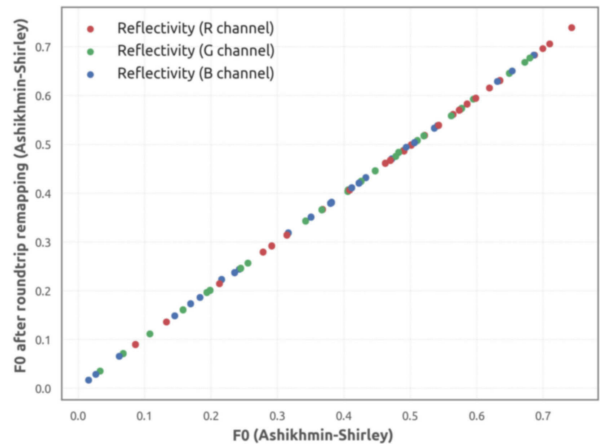


Figure 7: Round-trip remapping of conductors from Ashikhmin-Shirley to Ward and then back to Ashikhmin-Shirley. Remapped Fresnel coefficient F_0 vs original F_0 .

4.1.2. Dielectrics

The reflectance of dielectric materials includes an additional diffuse component. The specular component has a similar behaviour for all channels, and is usually approximated by a single parameter (e.g., the index of refraction). In Figure 8 we show the results of remapping from Ashikhmin-Shirley to Ward, using a simple optimisation with both diffuse and specular parameters. The plot corresponds to a parameter sweep of the IOR in Ashikhmin-Shirley for fixed diffuse and roughness parameters.

In this case, the instability signals a change of behaviour in the remapping process. In Figure 9 we show renderings that correspond

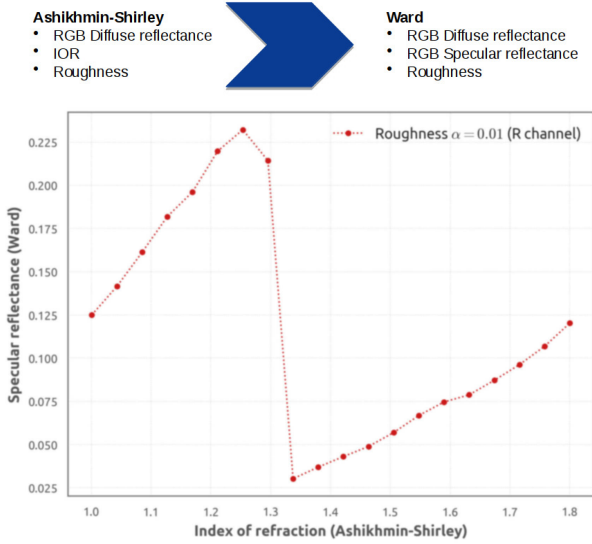


Figure 8: Simple remapping of dielectrics from Ashikhmin-Shirley to Ward. Detail of parameters in Mitsuba for both models, and plot of specular reflectance (Ward) vs IOR (AS).

to the points at both sides of the jump in the curve of Figure 8. In one case the remapping is working correctly, and we obtain a similar appearance in both models. In the other we observe that the optimisation arrives at a local minimum and the remapping is unable to recover the characteristic highlight from the source.

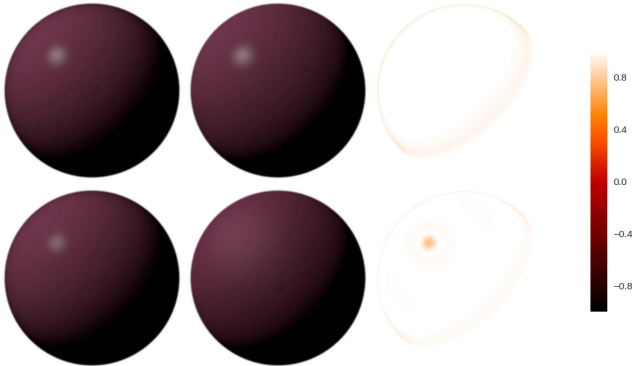


Figure 9: Source model (left), remapped target (center) and SSIM error (right), corresponding to $IOR = 1.3$ (top) and $IOR = 1.34$ (bottom) in Figure 8.

Figures 10 and 11 show the results of the two- and three-stage approaches, developed to improve the stability of the remapping process and illustrated on the diagrams of Figures 4 and 5. The two-stage approach effectively recovers a smooth relationship between the parameters, by avoiding the coupling between the diffuse and specular terms. With the additional optimisation step of the three-stage approach, in some cases we were able to slightly reduce the optimisation error with respect to the two-stage approach, but unfortunately the coupling between diffuse and specular terms still

causes several instabilities which make this second approach unreliable. In summary, in order to generate a robust remapping we need to avoid the coupling of the diffuse and specular components, by remapping each term independently (two-stage method).

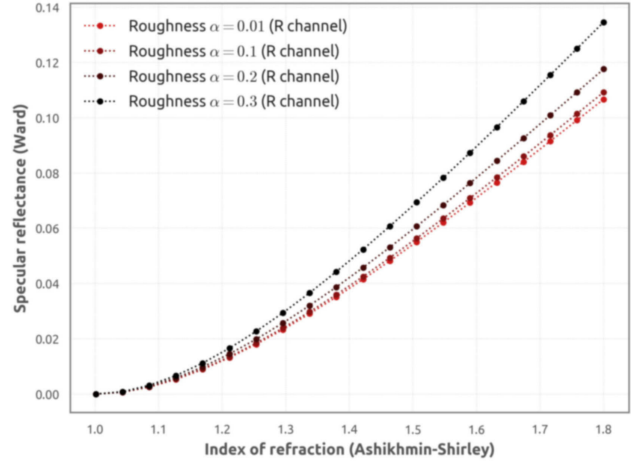


Figure 10: Two-stage remapping of conductors from Ashikhmin-Shirley to Ward. Specular reflectance vs Fresnel coefficient F_0 for multiple values of roughness.

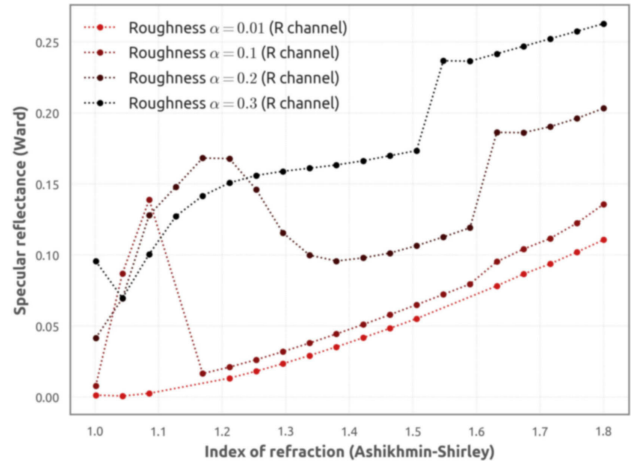


Figure 11: Three-stage remapping of conductors from Ashikhmin-Shirley to Ward. Specular reflectance vs Fresnel coefficient F_0 for multiple values of roughness.

5. Remapping of Spatially-Varying Materials

Spatially-varying materials are commonly defined using texture maps that provide the value of each model parameter across the surface. In Figure 12 we display the decomposition of an SVBRDF asset into texture maps describing four different parameters involved in the shading process (namely diffuse reflectance, specular roughness, specular reflectance, and surface normals).

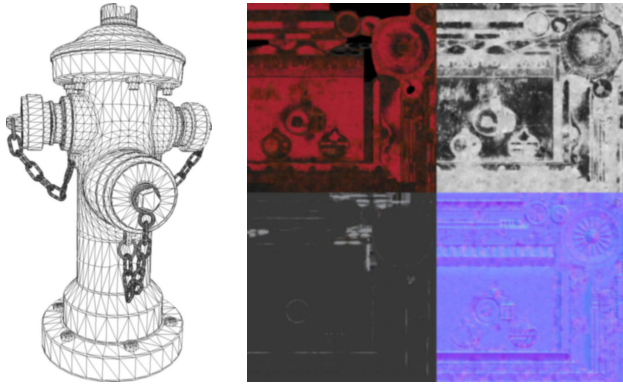


Figure 12: Decomposition of 3D asset into a low-resolution geometry and four texture maps describing the spatially-varying parameters of the material (diffuse reflectance, roughness, specular reflectance and normals).

The remapping of the corresponding spatially-varying material to a different BRDF model or renderer requires the remapping of each individual texel, which can be performed using one of the schemes for uniform BRDF remapping from the previous section. However, the optimisation required by the remapping of a single material usually takes a few minutes, which is acceptable for uniform BRDFs but intractable for high-resolution texture maps with hundred-thousands of texels.

To solve this problem we employ a regression scheme that utilises the data from the remapping of uniform materials to learn the relationship between parameters in both BRDF models involved. Through parameter sweep over the source model we generate a database of uniform material parameters and their remapped counterparts in the target model, which is used as input for a regression scheme. Thus we are able to generate a reduced representation of the transformation between the two models, which can then be evaluated efficiently without the need for further optimisation.

5.1. Parametric regression scheme

Figure 13 shows an example transformation that remaps between two implementations of Ward: from Mitsuba to Blender internal renderer. Due to established variations of well-known BRDF models, but also in order to address user expectations, such as energy preservation under changes of roughness, individual renderer implementations may take different design decisions, leading to differences between models despite having the same name.

The top plot shows a non-linear relationship between the two “roughness” parameters, illustrating a difference in implementations of Ward that cannot be explained by a simple rescaling of variables. The bottom plot offers a different set of cross-sections through the same remapping of parameter spaces: for a wide range of roughness values, we show how varying specular reflectance values of Mitsuba’s Ward map to Blender’s Ward model parameters. In contrast with the one-to-one correspondence between parameters found in the top plot, here the transformation traces a different mapping depending on the roughness parameter, signaling a complex rela-

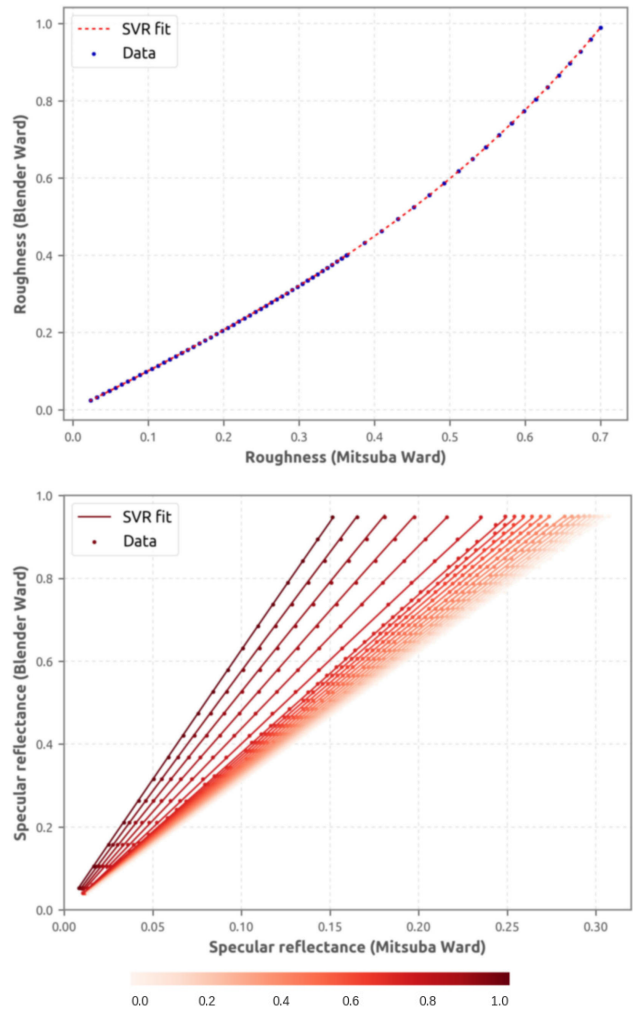


Figure 13: Remapping from Mitsuba-Ward to Blender internal-Ward, with data points and regression. *Top*: Remapping of roughness. The non-linear mapping shows that the two variants of Ward are distinct. *Bottom*: Remapping of specular reflectance with color indicating roughness. The transformation follows different mappings depending on the roughness parameter.

tionship between multiple parameters in the models which would be hard to recover by a manual mapping of model parameters.

The mapping of BRDF parameters of Figure 13 can be approximated by complex learning methods such as Support Vector Regression or Neural Networks. However, upon further scrutiny of the functional shape of the transformation, which presents common properties along different BRDF model pairs, we are able to formulate a parametric function able which capitalizes on these properties and is able to model the behaviour of the transformation with only a few parameters. Below we analyse the properties of the transformations and formulate the parametric approach for regression. In Section 5.3 we will compare this approach with Support Vector Regression and show that, in addition to being easier to train, it

presents a much better extrapolation of BRDF parameters outside of the region sampled by the training set.

In the top plot in Figure 13 we observe that the remapping of the roughness parameter depends only on the roughness. This behaviour is easy to model with a simple univariate polynomial fit of low-degree (≤ 4). In contrast, the remapping of the specular parameter (bottom) depends on both the roughness and the specular parts, presenting a more complex functional for the regression. However, the complexity of the regression can be drastically reduced by observing that for a fixed value of roughness, the relationship between specular parameters results in a very low-degree polynomial. In particular, when the specular parameters are linearly related to the intensity of the BRDF lobe, the specular transformation results in straight lines. (in the case of the IOR, as seen in Figure 10, the non-linear change of variable of equation 1 can be used to recover the specular reflectance). Thus, our parametric model for the specular transformation results in:

$$s_2(s_1, \alpha_1) = k(\alpha_1) \cdot s_1 \quad (2)$$

where s and α refer to specular and roughness parameters, and the subindices 1 and 2 indicate original, and remapped, respectively. With this parametric model, all that we have to do is compute the slope of the curves for each value of roughness, and then use this data to fit the non-linear relationship $k(\alpha_1)$ between roughness and slope. This can be done with a univariate non-linear fit with few coefficients c , such as:

$$k(\alpha) = c_0 + c_1 e^{-c_2 \alpha} + c_3 e^{-c_4 \alpha^2} \quad (3)$$

5.2. Results of Cross-Renderer SVBRDF Remapping

In line with the results from previous sections, we now proceed by basing all BRDF transformations on the robust two-stage remapping that operates on diffuse and specular components independently. For each pair of BRDF models of interest, we generate a database of mutually corresponding uniform material parameters and use this as input for a regression scheme that learns the mapping between models. This generates a reduced representation of the transformation, which can be evaluated swiftly in any part of the parameter space and without further optimisation or interaction with the renderer. Note that, even though our uniform remapping implementation requires the target BRDF to be defined within Mitsuba, we can reverse the role of source and target in the regression process, thus implementing BRDF remappings in the opposite direction.

In Figure 13 we analysed the remapping between two implementations of Ward: from Mitsuba to Blender internal renderer. Once the compact representation of the transformation is generated, it can be used to perform the remapping of every texel in the parameter maps of an SVBRDF. In Figures 14 and 15 we display the roughness and specular maps for Mitsuba-Ward and their corresponding remapped versions in Blender internal-Ward.

As previously seen, the transformation of the roughness (Figure 13 top) depends only on the original roughness, and thus the remapping of a roughness texture map is essentially a tonemapping operation, as observed in Figure 14. In contrast the remapping of the specular parameter (Figure 13 bottom) depends on both the rough-

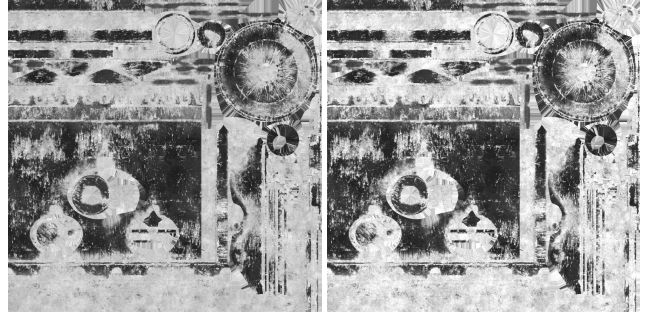


Figure 14: Roughness texture maps. *Left*: original Mitsuba's Ward. *Right*: remapped Blender's ward.

ness and the specular parts, which produces a remapped specular map that inherits details of the roughness map (Figure 15).

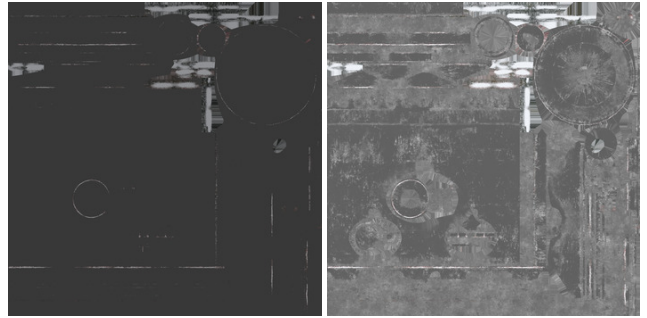


Figure 15: Specular texture maps. *Left*: original Mitsuba's Ward. *Right*: remapped Blender's ward.

Figure 16 displays the rendering of a 3D asset using the texture maps from Figures 14 and 15. The corresponding renderings show the efficacy of the remapping: faint visual differences are limited to surface parts that face both camera and light source. The bottom row shows specular in isolation, including an SSIM error image ($SSIM = 1$ indicates absolute similarity); removing the diffuse term, which is very similar across the renderers, highlights visual differences further.

Figure 17 displays a remapping from Mitsuba Ashikhmin-Shirley shader to Cycles' GGX model. Once again, we show cross-sectional plots of the parameter remapping function, as well as specular-only renderings with difference image. This result is of particular interest, as the specular lobe of GGX significantly differs from traditional microfacet models, such as Ashikhmin-Shirley. With its heavy tails, the specular term tends to add persistent sheen to a surface, making it challenging to match the appearance of a model with more compact reflectance lobes. Considering that, we believe that our remapping preserves the overall appearance exceptionally well.

Even within implementations of GGX, however, we observe slight differences between renderers, as can be seen in Figure 18 where we display a remapping from Mitsuba-GGX to Blender Cycles-GGX. Here the relationship between parameters is linear and only shows slight deviations from the identity transformation for the Fresnel coefficient F_0 . The simplest explanation for this behaviour is a small

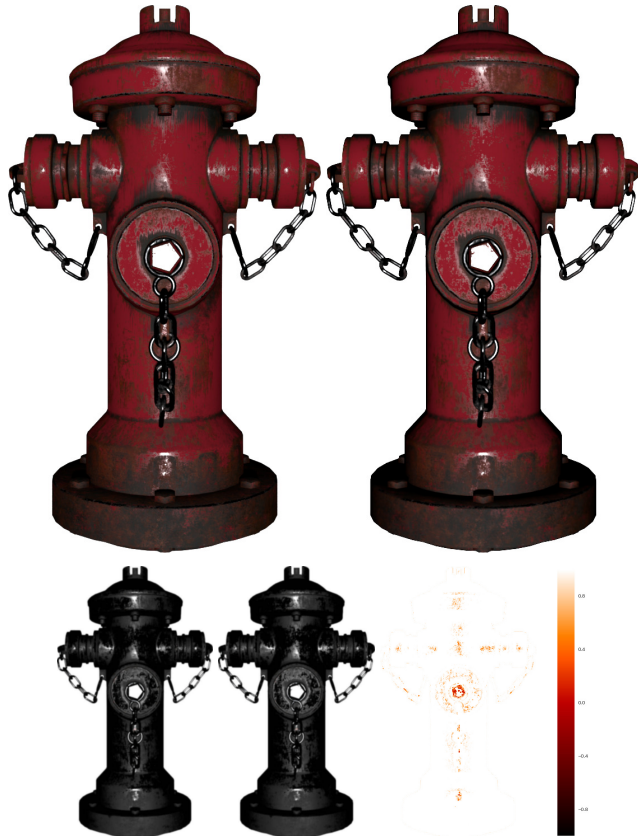


Figure 16: SVBRDF remapping from Mitsuba’s default Ward implementation to Ward within Blender’s internal renderer. *Top*: corresponding renderings using Mitsuba (*left*) and Blender (*right*). *Bottom*: specular-only renderings with SSIM error image determined in linear HDR ($SSIM = 1$ indicates absolute similarity).

difference in the parameterisation of F_0 in each model, although other contributions can not be discarded (e.g., small differences in the light sources in each renderer).

In general, we find the remapping scheme stable enough to enable chaining of transformations. Figure 19 shows an example transformation chain: Blender internal-Ward \rightarrow Mitsuba-Ward \rightarrow Mitsuba-GGX \rightarrow Blender Cycles-GGX, where the first transformation is the one depicted in Figure 13).

Apart from the inherently increased sheen due to GGX, the result remains remarkably close to the input. Note that in spite of working with three different renderers, the most noticeable differences occur when remapping from Ward to GGX within the same renderer (Mitsuba). This hints that the BRDF model shape is the main factor determining the remappability of a material, despite other additional differences that may be in play between renderers (e.g., source light behaviour, post-processing, etc.). In principle, the ability to chain transformations in this way allows to convert between a wide range of BRDF models and renderers without having to determine individual transformation for all possible pairs.

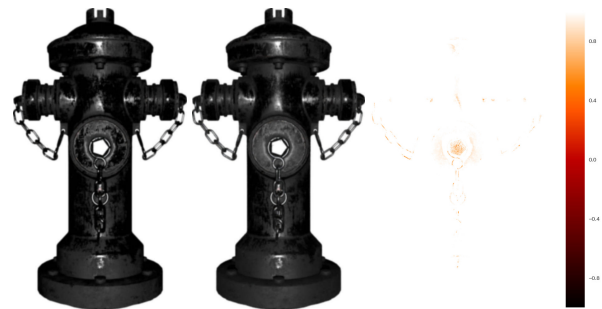
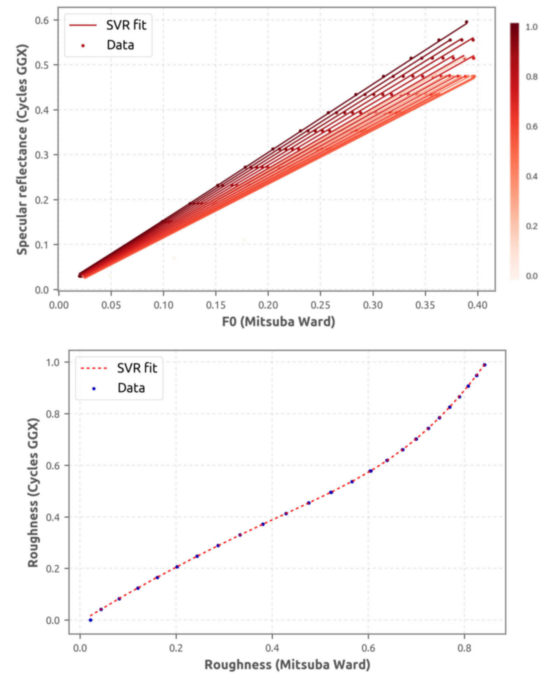


Figure 17: Remapping from Mitsuba Ashikhmin-Shirley to Cycles GGX. *Top*: remapping of Fresnel coefficient F_0 (left) with color indicating roughness, and remapping of roughness (right). *Bottom*: specular-only renderings with difference image.

5.3. Comparison with SVR

As mentioned in Section 5.1, the mapping between BRDF parameters can be learned using a regression method of general scope, without the need to make assumptions on the functional shape of the mapping. For the purpose of comparison we tested Support Vector Regression with radial basis functions, which requires an extra step of optimisation of the hyper-parameters through gradient-descent. Once trained, the SVR was able to correctly model and interpolate parameter values inside the region sampled by the training dataset, with equivalent results to our parametric approach in terms of SVBRDF remapping. The results of SVR remapping can be seen in Figure 16, where all the material parameters in the texture maps lie inside the subregion sampled by our dataset (i.e. the datapoints seen in Figure 13). However, when applying the SVR remapping to a general SVBRDF material which does not meet this requirement, we find that the SVR fails to extrapolate the behaviour of the

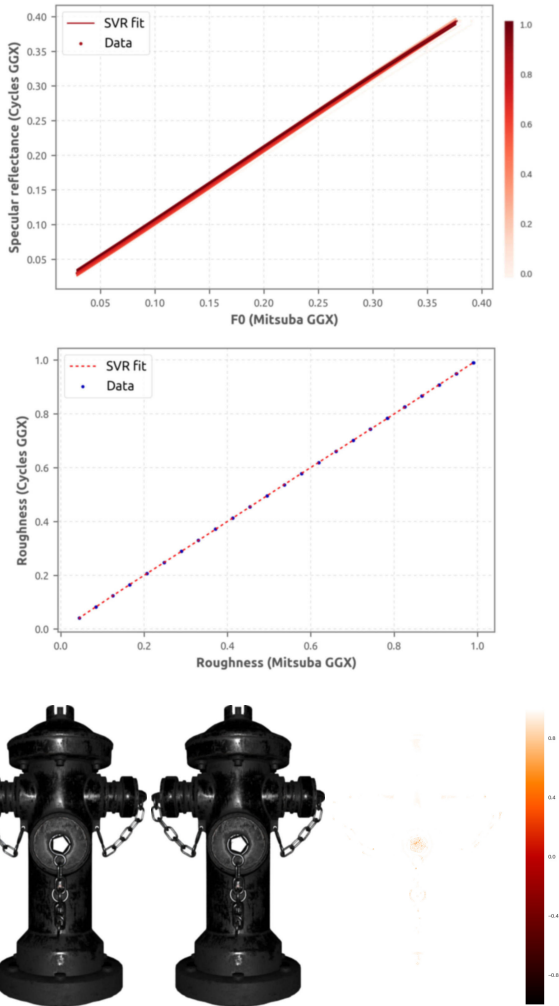


Figure 18: Remapping from Mitsuba GGX to Cycles GGX. *Top*: Remapping of Fresnel coefficient F_0 (left) with color indicating roughness, and remapping of roughness (right). *Bottom*: Specular-only renderings with SSIM error.

transformation outside of the sample space, thus generating fringe changes in the resulting asset. In Figure 21 we show the remapping of a spatially-varying material by means of both parametric (bottom-center) and SVR (bottom-right) regressions. The renderings use the environment map illumination from Figure 20.

Due to the extrapolation issues with SVR, the resulting remapping has suffered a very noticeable change in chromaticity. In contrast, the functional shape of our parametric function assumes a linear extrapolation of the specular values. This means that in the transformation of parameters, the three channels of each texel are multiplied by the same factor, thus leading to a conservation of the chromaticity.

5.4. Illuminant position

As previously discussed in Section 4.1, our scheme for uniform BRDF remapping utilises a rendered scene with point light illumina-

tion to provide a partial sampling of the material’s reflectance. The main requirement that we found for the light position during our experiments is that a great proportion of the pixels in the resulting renderings should be illuminated, so that the optimisation is able to converge and we obtain a stable transformation. This needs to happen for all considered combinations of parameters, including materials with low roughness where the highlight does not spread far from the direction of specular reflection. An obvious choice for this purpose is a lightsource concentric with the camera, which maximises the size of the specular highlight in the rendering, thus improving the characterisation of the lobe. However, the symmetry of the scene configuration poses multiple potential issues: (1) an over-representation of the retroreflective lobe in the sampling; (2) a repeated sampling of directions which in isotropic BRDFs are equivalent and do not provide new information; (3) for many BRDF models, insufficient coverage of the parameter space to constrain all parameters, for instance the Fresnel term.

In Figures 23-25 we display the remappings of spatially-varying materials with two different light settings: frontal light (top) and non-frontal light with $\theta_l = 45^\circ$ (bottom). Visual differences between these two settings for remapping are hard to spot, but in some cases a slight decrease of the global dissimilarity is apparent when using non-frontal light. This is confirmed by the plots in Figure 22 where we can observe the corresponding mean dissimilarity errors of these materials as we rotate the environment map illumination (note that we refer to a rotation of the illumination used for the renderings, *not* the one used in the remapping). Videos of these and other remappings with rotating environment illumination can be found in the supplemental material.

6. Conclusions

We presented a method for automatic translation of material appearance between different BRDF models and across different renderers, which uses an image-based metric for appearance comparison, and that delegates the interaction with the model to the renderer. We analysed the performance of the method, both with respect to robustness and visual differences of the fits for multiple combinations of BRDF models. While it is effective for individual BRDFs, the computational cost does not scale well for spatially-varying BRDFs. Therefore, we also presented an interpolation scheme based on a non-linear parametric regression of the transformation between BRDF model. We used this to generate a reduced polynomial representation of the transformation which evaluates instantly and without further interaction with the renderer, allowing the remapping of SVBRDF texture maps. Moreover, the resulting transformations lend themselves to chaining, enabling effortless transitions between BRDF models. We compared our regression scheme with Support Vector Regression and showed that it provides a better extrapolation of model parameters outside of the area defined by the training data. Finally we analysed the effect of the lighting used during uniform remapping in the quality of renderings of spatially-varying materials, and confirmed that headlight illumination leads to a slight increase in visual differences.

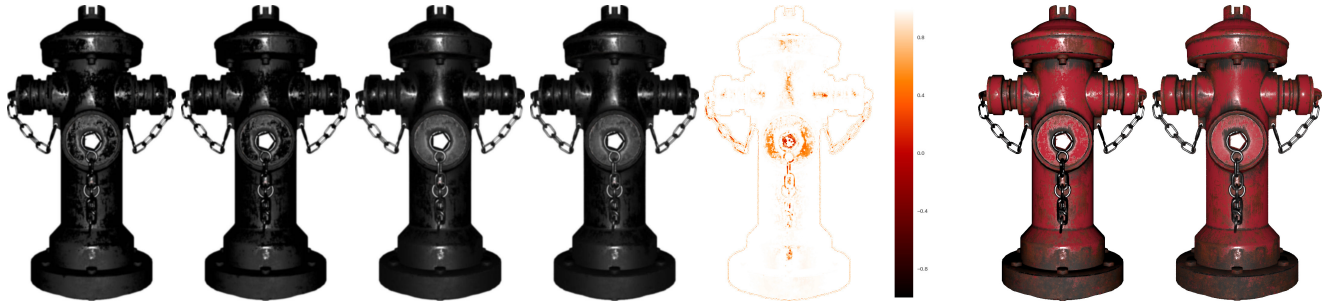


Figure 19: Chained remapping from Ward (Blender) to GGX (Cycles) via two intermediate BRDF models. *Left to right*: Blender internal-Ward, Mitsuba-Ward, Mitsuba-GGX, Blender Cycles-GGX, SSIM error. *With diffuse term*: Blender internal-Ward, Blender Cycles-GGX.



Figure 20: Tabac plant environment map.

References

- [All17] Allegorithmic: Substance designer and substance painter. <https://www.allegorithmic.com>, 2017. Last access Oct. 2017. 2
- [AS00] ASHIKHMINS M., SHIRLEY P.: An anisotropic phong brdf model. *J. Graph. Tools* 5, 2 (Feb. 2000), 25–32. 2
- [BLPW14] BRADY A., LAWRENCE J., PEERS P., WEIMER W.: gen-BRDF: Discovering new analytic BRDFs with genetic programming. *ACM Trans. Graph.* 33, 4 (July 2014), 114:1–114:11. 1
- [Bur12] BURLEY B.: Physically-based shading at disney. In *ACM SIGGRAPH 2012 Courses* (2012), SIGGRAPH '12. 2
- [Cor17] Corona renderer. <https://corona-renderer.com>, 2017. Last access Oct. 2017. 2
- [Dam17] DAMEZ C.: Personal communication (CTO, Allegorithmic), Oct. 2017. 2
- [DHT*00] DEBEVEC P., HAWKINS T., TCHOU C., DUIKER H.-P., SAROKIN W., SAGAR M.: Acquiring the reflectance field of a human face. In *Proceedings of the 27th Annual Conference on Computer Graphics and Interactive Techniques* (New York, NY, USA, 2000), SIGGRAPH '00, ACM Press/Addison-Wesley Publishing Co., pp. 145–156. 3
- [GGG*16] GUARNERA D., GUARNERA G., GHOSH A., DENK C., GLENCROSS M.: BRDF representation and acquisition. *Comput. Graph. Forum* 35, 2 (May 2016), 625–650. 1, 2
- [HFM16] HAVRAN V., FILIP J., MYSZKOWSKI K.: Perceptually Motivated BRDF Comparison using Single Image. *Computer Graphics Forum* (2016). 2
- [Jak10] JAKOB W.: Mitsuba renderer, 2010. <http://www.mitsuba-renderer.org>. 3
- [Kri17] KRIVANEK J.: Personal communication (Head of Research, Corona Renderer), Jul. 2017. 2
- [LFTG97] LAFORTUNE E. P. F., FOO S.-C., TORRANCE K. E., GREENBERG D. P.: Non-linear approximation of reflectance functions. In *Proceedings of the 24th Annual Conference on Computer Graphics and Interactive Techniques* (New York, NY, USA, 1997), SIGGRAPH '97, ACM Press/Addison-Wesley Publishing Co., pp. 117–126. 2
- [Mar98] MARSCHNER S. R.: *Inverse Rendering for Computer Graphics*. PhD thesis, Cornell University, Ithaca, NY, 1998. 2
- [May17] Autodesk maya. <https://www.autodesk.com/products/maya>, 2017. Last access Oct. 2017. 2
- [NDM05] NGAN A., DURAND F., MATUSIK W.: Experimental analysis of BRDF models. In *Proceedings of the Sixteenth Eurographics Conference on Rendering Techniques* (Aire-la-Ville, Switzerland, Switzerland, 2005), EGSR '05, Eurographics Association, pp. 117–126. 2
- [NDM06] NGAN A., DURAND F., MATUSIK W.: Image-driven navigation of analytical brdf models. In *Proceedings of the 17th Eurographics Conference on Rendering Techniques* (Aire-la-Ville, Switzerland, Switzerland, 2006), EGSR '06, Eurographics Association, pp. 399–407. 2, 3
- [PJH16] PHARR M., JAKOB W., HUMPHREYS G.: *Physically Based Rendering, Third Edition: From Theory To Implementation*, 3rd ed. Morgan Kaufmann Publishers Inc., San Francisco, CA, USA, 2016. 2
- [SDSG13] SCHREGLE R., DENK C., SLUSALLEK P., GLENCROSS M.: Grand Challenges: Material Models in the Automotive Industry. In *Eurographics Workshop on Material Appearance Modeling* (2013), Klein R., Rushmeier H., (Eds.), The Eurographics Association. 1
- [Uni17] Unity. <https://unity3d.com/>, 2017. Last access Oct. 2017. 2
- [Unr17] Unreal engine. <https://www.unrealengine.com>, 2017. Last access Oct. 2017. 2
- [WLL*08] WEYRICH T., LAWRENCE J., LENSCH H., RUSINKIEWICZ S., ZICKLER T.: Principles of appearance acquisition and representation. *Foundations and Trends in Computer Graphics and Vision* 4, 2 (2008), 75–191. 2
- [WMLT07] WALTER B., MARSCHNER S. R., LI H., TORRANCE K. E.: Microfacet models for refraction through rough surfaces. In *Proceedings of the 18th Eurographics Conference on Rendering Techniques* (Aire-la-Ville, Switzerland, Switzerland, 2007), EGSR'07, Eurographics Association, pp. 195–206. 2
- [WMP*06] WEYRICH T., MATUSIK W., PFISTER H., BICKEL B., DONNER C., TU C., MCANDLESS J., LEE J., NGAN A., JENSEN H. W., GROSS M.: Analysis of human faces using a measurement-based skin reflectance model. *ACM Trans. Graph. (Proc. SIGGRAPH)* 25, 3 (July 2006), 1013–1024. 3

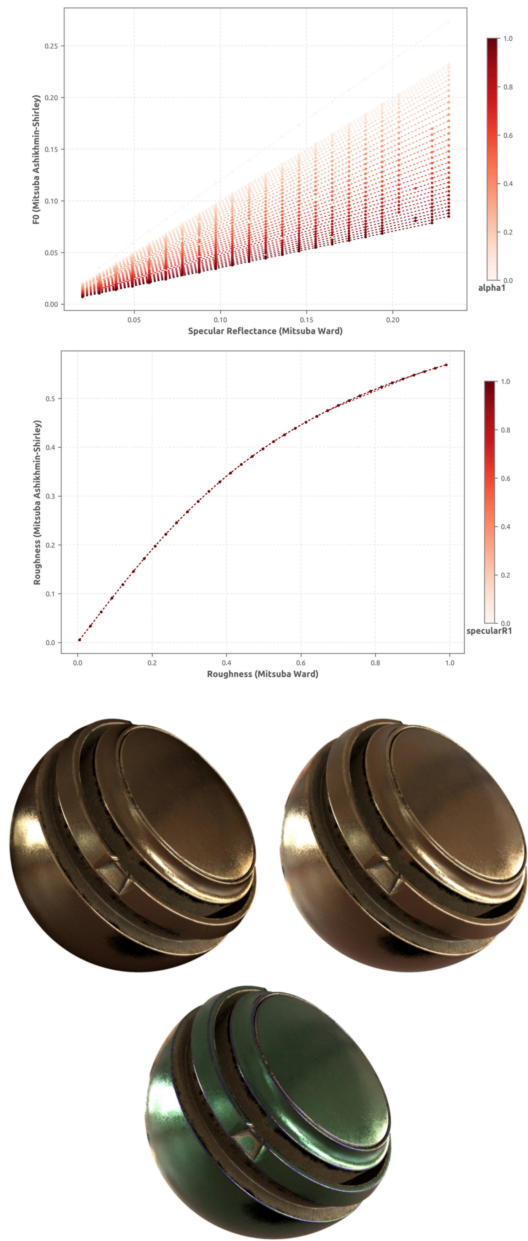


Figure 21: *Plots*: Remapping from Mitsuba Ward to Mitsuba Ashikhmin-Shirley. Remapping of specular reflectance with color indicating roughness, and remapping of roughness. *Renderings*: Renderings of the remapping of a spatially-varying material (*scratched gold*) using two different methods for regression. Left: original Mitsuba-Ward. Right: remapped Mitsuba Ashikhmin-Shirley with our parametric scheme. Bottom: remapped Mitsuba Ashikhmin-Shirley with Support Vector Regression. Illumination is provided by the environment map from Figure 20.

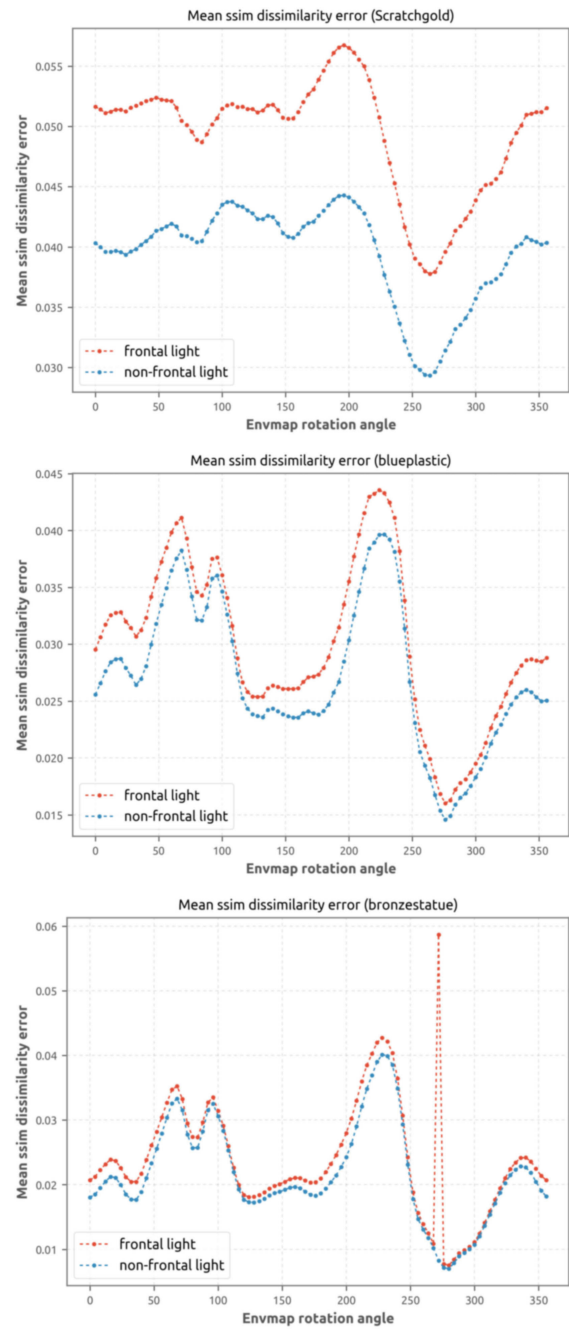


Figure 22: Mean dissimilarity error ($1 - \text{SSIM}$) for three SVBRDF materials as a function of the rotation angle of the illuminating environment map from Figure 20. Higher values indicate higher error. *Top*: scratched gold. *Center*: blue plastic. *Bottom*: Bronze statue. Remapping scene with headlight (red) and non-headlight illumination (blue).

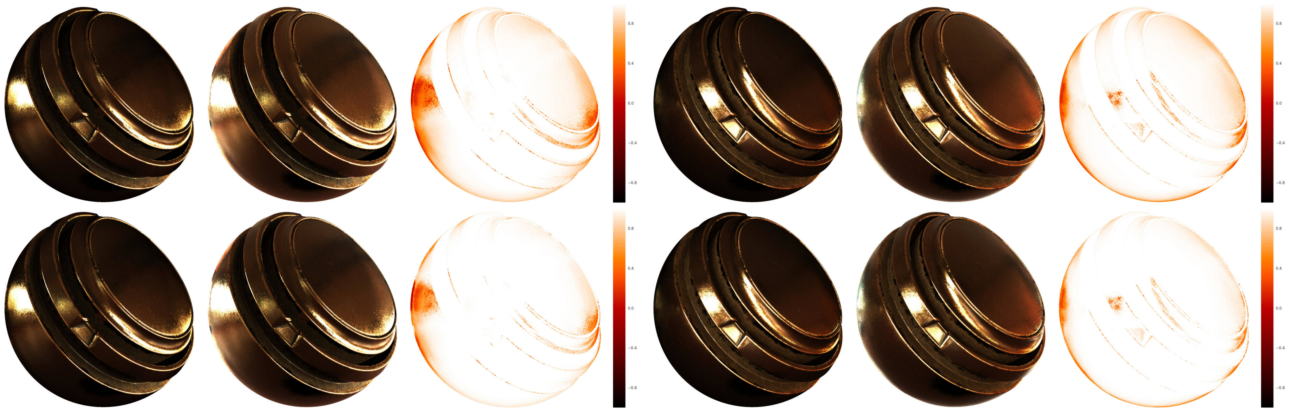


Figure 23: Remappings of scratched gold with frontal (top) and non-frontal light (bottom). Illumination provided by environment map from Figure 20 at rotation angles 0° (left side) and 272° (right side). Within each side: *Left*: original material in Mitsuba Ward. *Center*: remapped in Mitsuba Ashikhmin-Shirley. *Right*: SSIM difference.

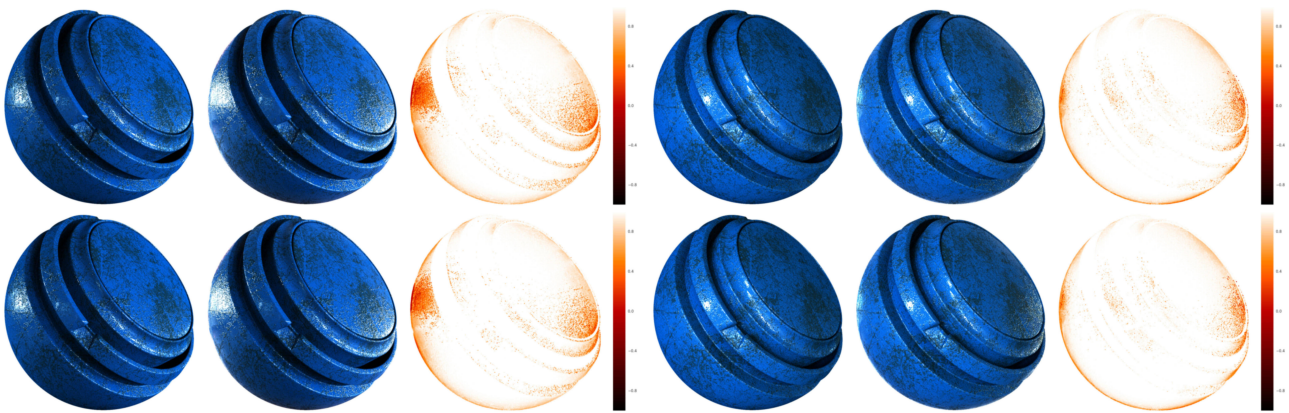


Figure 24: Remappings of blue plastic with frontal (top) and non-frontal light (bottom). Illumination provided by environment map from Figure 20 at rotation angles 0° (left side) and 272° (right side). Within each side: *Left*: original material in Mitsuba Ward. *Center*: remapped in Mitsuba Ashikhmin-Shirley. *Right*: SSIM difference.

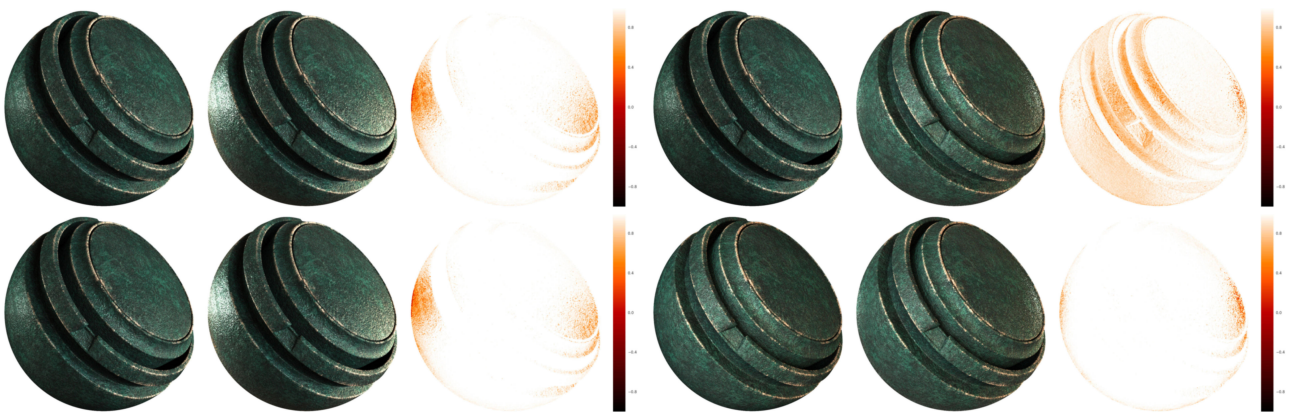


Figure 25: Remappings of bronze statue with frontal (top) and non-frontal light (bottom). Illumination provided by environment map from Figure 20 at rotation angles 0° (left side) and 272° (right side). Within each side: *Left*: original material in Mitsuba Ward. *Center*: remapped in Mitsuba Ashikhmin-Shirley. *Right*: SSIM difference.